Frequency noise optimization in micromachined resonant sensors

Theo Miani
Silicon Microgravity
Cambridge, UK
tmiani@silicong.com

Lokesh Gurung
Silicon Microgravity
Cambridge, UK
lgurung@silicong.com

Guillermo Sobreviela-Falces
Silicon Microgravity
Cambridge, UK
gsobreviela@silicong.com

Douglas Young
Silicon Microgravity
Cambridge, UK
dyoung@silicong.com

Niall MacCarthy
Silicon Microgravity
Cambridge, UK
nmaccarthy@silicong.com

Colin Baker
Silicon Microgravity
Cambridge, UK
cbaker@silicong.com

Ashwin Seshia
Cambridge University
Cambridge, UK
aas41@cam.ac.uk

***Abstract*— We present the results of improved front end electronic for low-noise MEMS vibrating beam accelerometers (VBAs). We introduce a theoretical model to improve the frequency noise by taking advantage of relative difference between uncorrelated additive noise sources. Experimental results demonstrate the improvement of the frequency noise following the prediction of the model. This results in the demonstration of 50 % reduction of the integrated frequency noise over 100 Hz bandwidth.**

Keywords—Vibrating beam accelerometer, oscillators, frequency noise.

I. Introduction

Micromachined resonant sensors often operate on the principle of tracking shifts in resonant frequencies of one or more vibrating elements. The continuous tracking of resonant frequencies is aided by the implementation of a closed-loop oscillator front-end interface. The optimization of this front-end interface is critical to addressing key specifications such as sensor resolution and stability. This paper addresses the understanding of the interplay of various noise sources in this interface and their shaping by response blocks in the loop including the mechanical resonator. The insights derived from this model are then applied to the optimization of the PSD of a purpose-built oscillator circuit for high-end micromachined resonant sensors [1]. In open-loop configurations, the phase noise is closely linked to additive noise [2]. Closed-loop operation introduces a corner frequency, connected to the resonant frequency and quality factor of the beam, influencing the integration of phase noise [3]. The resolution of the resonant sensor is directly connected to the noise integrated within the sensor bandwidth [4], highlighting the importance of considering this corner frequency. Our research addresses a domain where the limits are influenced by resonator input noise. Through achieving a relative reduction in electronic noise compared to resonator input noise, we demonstrate the capacity to extend the corner frequency and diminish the overall noise integrated within the bandwidth according to the mathematical Lesson's model [5].

II. Theory

The resonant sensor presented is a vibrating beam both actuated and sensed using capacitive transduction. The actuation is performed by an input voltage V_{in} applied to the drive electrode. Due to electrostatic force the vibrating beam move and generates a motional current I_m in the sense electrode. A Trans Impedance Amplifier (TIA) is used to convert the motional current to an output voltage V_{out} through a feedback resistance R_f. Additive noise is the dominant from the noise contribution. Figure 1 (a) presents the schematic of the front-end electronics and its associated additive noises. An impedance in the TIA input R_{load} is added to the schematic, which represents the vibrating beam motional impedance, or a resistor placed to emulate this motional impedance. These two configurations are important in the understanding of the additive noise sources. An additive noise $E_{R_{load}}$ is associated to the impedance of the TIA input. In the case this impedance is a resistor, its associated noise represents the Johnson noise of the resistor. In the case of vibrating beam motional impedance this noise represents the Brownian noise reported in the input of the vibrating beam. E_{R_f} is the Johnson noise of the feedback resistor. I_n and I_p are the equivalent input current noise of the TIA. E_p is the equivalent input voltage noise of the TIA.

Figure 1 (b) plots the measured Power Spectral Density (PSD) of the additive noises, in blue in the case of resistor and in red in the case of the vibrating beam motional impedance. A 55 kΩ resistor is used to match the motional resistance of the vibrating beam. Both measurements are performed using Zurich Instrument Lock-in Amplifier (LIA). A gain stage of 7.3 is added to the set-up. On one hand, the LIA tracks and measures the resonance of the vibrating beam during 20 minutes. On the other hand, the LIA applied the frequency

of 110 kHz, which matches the vibrating beam resonance, and measures the output of the TIA. In both cases the amplitude signal is processed, and its PSD is calculated.

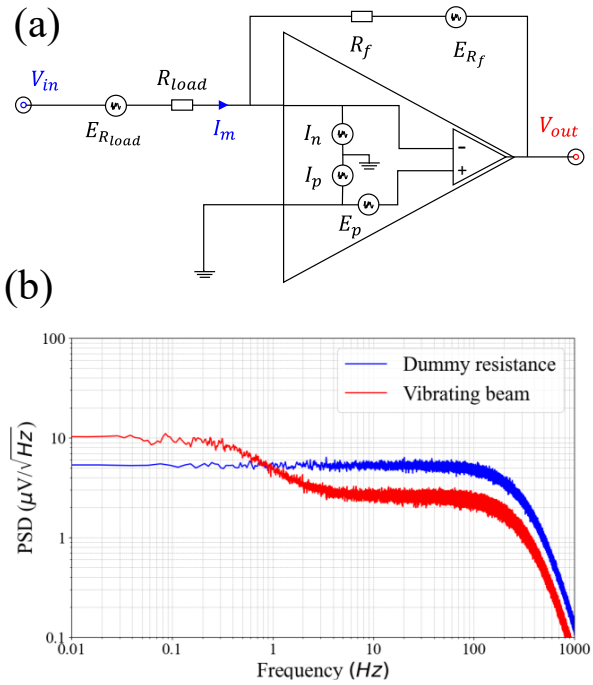

Figure 1: (a) Block diagram of front end electronic with its dominant noise source. (b) Additive noise spectrum of the front end electronics using (blue) a dummy resistance load, and (red) the resonator as a load.

The PSD of the two experiments show different shapes. Table 1 details the additive noise sources of the resistor experiment, expressed on the output node V_{out}. In this configuration the Johnson noise of the resistor $E_{R_{load}}$ is the dominant noise source following by the Johnson noise of the feedback resistance E_{Rf}. The total noise of the noise model matches with the floor noise measured experimentally.

Table 1 - additive noise of the dummy resistance experiment

Additive noise	Output node	Value
$E_{R_{load}}$	$E_{R_{load}} \frac{R_f}{R_{load}}$	$4.4\mu V/\sqrt{Hz}$
E_{R_f}	E_{R_f}	$2.03\mu V/\sqrt{Hz}$
$I_{n,p}$	$I_n R_f$	$0.08\mu V/\sqrt{Hz}$
E_p	$E_p\left(1+\frac{R_f}{R_{load}}\right)$	$0.16\mu V/\sqrt{Hz}$
E_{tot}	$\sqrt{\sum E^2}$	$4.85\mu V/\sqrt{Hz}$

Table 2 details the additive noise sources of the vibrating beam experiment, expressed on the output node V_{out}. In this configuration the Johnson noise of the feedback resistance E_{R_f} is dominant. The total noise of the noise model matches with the floor noise measured experimentally after 5 Hz.

Table 2 – additive noise of the vibrating beam experiment.

Additive noise	Output node	Value
E_{R_f}	E_{R_f}	$2.03\mu V/\sqrt{Hz}$
$I_{n,p}$	$I_n R_f$	$0.08\mu V/\sqrt{Hz}$
E_p	E_p	$0.03\mu V/\sqrt{Hz}$

Indeed, the shape of the additive noise of the vibrating beam highlights key features. A first-floor noise is observed at low frequency (<0.1 Hz) and then filtered around 0.5Hz to reach a second-floor noise at higher frequency (>5Hz). Because the vibrating beam has a 110 kHz resonance frequency and 100,000 Quality factor, this 0.5 Hz frequency corresponds to the vibrating beam cut off frequency. This noise floor represents an input noise of the vibrating beam which is filtered by the mechanical response of the beam resonance.

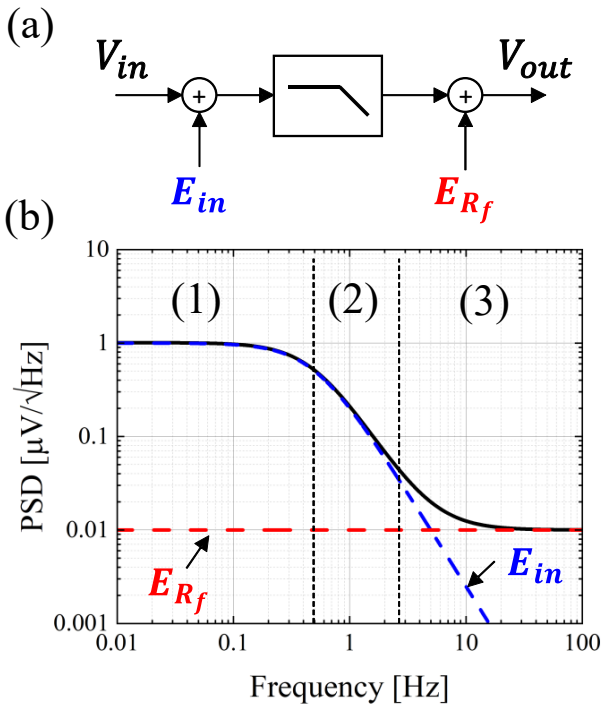

Figure 2: (a) Block diagram of additive noises. The resonator input noise, denoted as E_{in}, acting on the vibrating beam input V_{in}. The electrical noise can be modeled as an output noise, represented by E_{R_f}, on the vibrating beam output V_{out}. Around the carrier frequency, the vibrating beam is modeled as a low-pass filter. (b) Additive noise PSD, highlighting the resonator input noise in blue and the electrical noise in red.

Figure 2 (a) illustrates two of the key noise sources in the loop including resonator input noise and Johnson noise of

the feedback resistance. The Trans-Impedance Amplifier's (TIA) electronic noise, dominated by the feedback resistance Johnson noise E_{Rf}, is treated as additive and uncorrelated to the resonant beam output. Simultaneously, vibrating beam noise acts as an input noise term, filtered by the transfer function of the resonant element. Figure 2(b) displays the Power Spectral Density (PSD) of the additive noise around the carrier frequency, highlighting three frequency domains: (1) where input noise dominates, (2) the domain of filtered input noise, and (3) where electronic noise surpasses filtered input noise. The corner frequency between (2) and (3) depends on the relative magnitudes of these noise sources.

Figure 3(a) demonstrates how the phase noise, proportional to the Signal to Noise Ratio (SNR), can be modelled in the closed-loop system. Due to the closed loop, phase noise is reinjected into the input of the vibrating beam and is shaped by the resonator and amplifier gain blocks in the loop. Figure 3(b) demonstrates how the relative difference between input and output noise influences the corner frequency of phase noise integration. In domain (1), the frequency noise is limited by input noise. In domain (2), the frequency noise is integrated but appears flat due to domination by the filtered input noise. In domain (3), the frequency noise is limited by electronic noise, allowing integration.

(a)

$$S_\phi(\omega) = S_{\phi_0}(\omega)\frac{1}{\left(1-\frac{\omega_1}{\omega_2}\right)^2}\left(1+\left(\frac{\omega_2}{\omega}\right)^2\right)$$

(b)

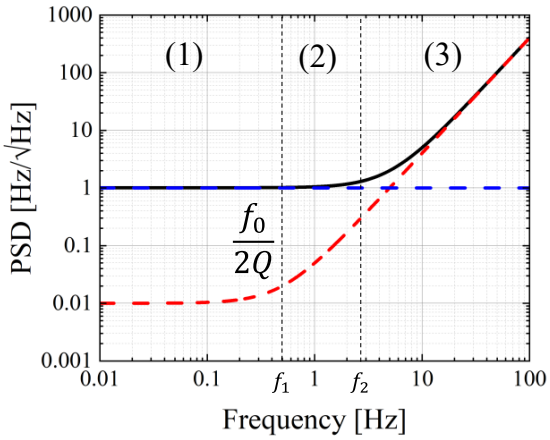

Figure 3: (a) Attenuated phase noise S_ϕ when a LPF with finite attenuation is applied [5]. ω_1 and ω_2 are respectively the corner frequency between (1) and (2) and (2) and (3). The phase noise S_{ϕ_0} is attenuated by the ω_1/ω_2 ratio and ω_2 acts as the corner frequency. (b) Frequency noise PSD (phase noise $\times\ \omega$), highlighting the cutoff frequency of the attenuated phase noise appearing after the vibrating beam corner frequency ($\omega_1 = 2\pi f_0/2Q$). (1), (2), and (3) denote, respectively, the frequency domains where input noise dominates, where it is filtered, and where the electrical noise dominates.

III. Experiment

The aim of the experiment is to prove by improving the relative difference between the additive noise sources the corner frequency of the frequency noise can be improved. The Johnson noise of the feedback resistance can be improved by increasing the value of the feedback resistance. The experiment consists of reproducing the measurement performed on Figure 1 for 3 different values of feedback resistance. Changing the feedback resistance will both change the Johnson noise associated E_{R_f} in addition to the signal transduction, which is the product of $I_m \times R_f$. To compare the relative differences between the two noise sources, the additive noise PSD is calculated relative to the signal amplitude.

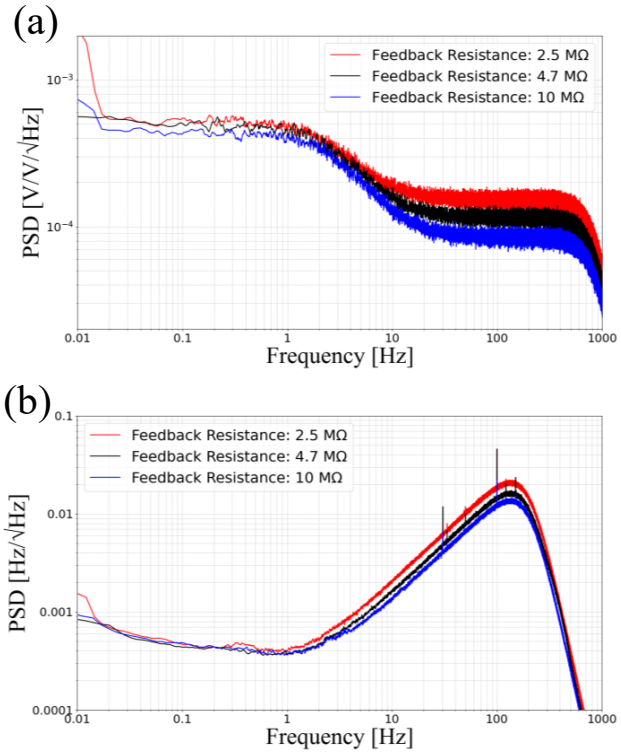

Figure 4: (a) Relative additive noise PSD expressing the PSD of additive noise relatively to the amplitude of the signal. In blue, black and red the additive noises for respectively 500kΩ, 5MΩ and 50 MΩ feedback resistance. After 5 Hz there are some spurious peaks resulting to the closed loop system but that don't affect the sensor output. (b) Frequency noise PSD. In blue, black and red the acceleration noises for respectively 500kΩ, 5MΩ and 50 MΩ feedback resistance. After 30Hz there are some spurious peaks resulting to ambient vibration

Figure 4 (a) shows the measured additive noise PSD as the feedback resistance is increased from 2.5 MΩ to 10 MΩ. Because the input noise level stays constant relative to the feedback resistance, these noise sources are decoupled from the output noise sources. Figure 4 (b) shows this effect in the frequency PSD for the same experiment: The corner frequency where the noise is integrated increases by increasing the feedback resistance. However, the floor noise before the corner frequency stay the same. The floor noise of the frequency PSD is not improving by the feedback resistance increase because it is limited by the input additive noise. The improvement of this method is the reduction of the integrated noise in a fixed bandwidth. Table 1 shows the integrated frequency noise over 100 Hz of bandwidth for the different feedback resistance used.

Table 3 – comparison of the integrated frequency noise according to the used feedback resistance

Feedback resistance	2.5 MΩ	4.7 MΩ	10 MΩ
Johnson noise	155 $\mu V/\sqrt{Hz}$	115 $\mu V/\sqrt{Hz}$	85 $\mu V/\sqrt{Hz}$
Integrated noise	4.1 Hz	3.23 Hz	2.68 Hz

IV. Conclusion

The understanding of the limiting additive noise source in resonant sensors allows improving the integrated noise of the system. For a fixed bandwidth (@100 Hz) the increase of feedback resistance by a factor of 4 improved the integrated noise by 50 % without affecting other performance parameters. However, the increase of the feedback resistance of the TIA is limited by the gain product bandwidth of the TIA. Operating beyond this product will affect the SNR of the sensor and degrade the floor noise of the system. The input noise of the resonant sensor is limited by the thermomechanical noise of the beam and the bias voltage of the sensor.

References

[1] [1] L. Gurung, T. Miani, G. Sobreviela-Falces, D. Young, C. Baker and A. Seshia, "A high-performance resonant MEMS accelerometer with a residual bias error of 30 µg and scale factor repeatability of 2 ppm," *2023 IEEE International Symposium on Inertial Sensors and Systems (INERTIAL)*, Lihue, HI, USA, 2023

[2] T. Miani *et al*., "Nanoresonator-based accelerometer with large bandwidth and improved bias stability," *2022 IEEE International Symposium on Inertial Sensors and Systems (INERTIAL)*, Avignon, France, 2022

[3] D. B. Leeson, "A simple model of feedback oscillator noise spectrum," in *Proceedings of the IEEE*, vol. 54, no. 2, pp. 329-330, Feb. 1966, doi: 10.1109/PROC.1966.4682.

[4] R. Levy and V. Gaudineau, "Phase noise analysis and performance of the Vibrating Beam Accelerometer," *2010 IEEE International Frequency Control Symposium*, Newport Beach, CA, USA, 2010

[5] G. Sauvage, "Phase Noise in Oscillators: A Mathematical Analysis of Leeson's Model," in *IEEE Transactions on Instrumentation and Measurement,* vol. 26, no. 4, pp. 408-410, Dec. 1977, doi: 10.1109/TIM.1977.4314586.